Shap. Mem. Superelasticity
https://doi.org/10.1007/s40830-020-00273-3

ICFSMA 2019

Systematic Trends of Transformation Temperatures and Crystal Structure of Ni–Mn–Ga–Fe–Cu Alloys

Andrew Armstrong[1,2] · Frans Nilsén[2] · Michal Rameš[2] · Ross H. Colman[3] · Petr Veřtát[2] · Tomáš Kmječ[3] · Ladislav Straka[2,3] · Peter Müllner[1] · Oleg Heczko[2]

Abstract Here we report a systematic research on effects of Fe and Cu upon properties relevant for the magnetic shape memory effect of Ni–Mn–Ga ferromagnetic shape memory alloys. Fe and Cu were identified as elements with potential synergism to increase the martensite transformation temperature of Ni–Mn–Ga magnetic shape memory (MSM) alloys. Eighteen Ni–Mn–Ga–Fe–Cu alloys with different systematic trends in substituting the ternary elements with Cu and Fe have been investigated. We found a method to describe the effectiveness of Ni, Mn, and Cu upon raising the martensitic transformation temperature, lowering the saturation magnetization, and varying the Curie temperature. We find the martensite transformation temperature most influenced by the Ni content, followed by Mn, with a smaller effect of Cu. The saturation magnetization decreases with similar coefficients for Mn and Cu alloying. The Curie temperature monotonously decreases with Mn, but not Cu. The 10M martensite structure is stable for the composition $Ni_{46.5}Mn_{25+X}Ga_{25-X-Y}Fe_{3.5}Cu_Y$ with X and Y range of 0–5.7, and 0.8–3.0. Used in combination with the *total e/a*, the *elemental e/a-ratio* gives some insight into the complex behavior of quinary MSM alloys and is a useful method of analyzing MSM alloys for improved functional properties.

Introduction

Magnetic shape memory (MSM) alloys actuate in response to magnetic fields [1]. They convert magnetic field energy into large-strain (up to 12%) high-speed ($\sim$ 1–10 ms) reversible deformation with work-output approximately 2.6×10^4 J/m^3 [2]. MSM alloys can expand, contract, and bend in response to magnetic fields [3–5]. The mechanical degrees of freedom of axial strain and bending [6] allows for complex motion, such as for small constrictions that can be swept through the material in the case of MSM micropumps [7, 8]. MSM alloys absorb energy in the motion of their twin boundaries and can be used as dampers [9, 10] and energy harvesters [11]. In short, MSM alloys behave akin to metallic muscles activated by magnetic field, morphing to a variety of geometries, and can operate down to cryogenic temperatures as low as 2 K [12].

Three martensite structures are stable in Ni–Mn–Ga MSM alloys: five-layer modulated (10M); seven-layer modulated (14M); and non-modulated (NM) [13–17]. The 10M phase exhibits very low twinning stress ($\approx$ 0.1–1 MPa) [18], making it efficient for magnetic actuation. The maximum operating temperature is, however, often the limiting factor for 10M actuators; aerospace applications, for example require operation up to 373 K [19]. Pagounis et al. [20] found the highest austenite start temperature for 10M alloy (i.e., maximum operating

ICFSMA 2019 Credit Line: This article is an invited submission to *Shape Memory and Superelasticity* selected from presentations at the International Conference on Ferromagnetic Shape Memory Alloys (ICFSMA) held June 2–7, 2019 in Prague, Czech Republic, and has been expanded from the original presentation. (Gray header bar: ICFSMA 2019).

✉ Andrew Armstrong
andrewarmstrong858@u.boisestate.edu

[1] Micron School of Materials Science and Engineering, Boise State University, Boise, ID 83725, USA

[2] Institute of Physics, Czech Academy of Sciences, Na Slovance, 1999/2, 182 21 Prague 8, Czech Republic

[3] Faculty of Mathematics and Physics, Charles University, Ke Karlovu 2026/5, 121 16, Prague 2, Czech Republic

Published online: 03 March 2020

temperature) which was 353 K in $Ni_{50.8}Mn_{28.4}Ga_{20.8}$ alloy. In this study, we sought to increase the temperature of martensitic transformation (T_M) of the 10M phase through combined Fe and Cu alloying.

One can modify the operational temperature in Ni–Mn–Ga MSM alloy by alloying, as the T_M is sensitive to elemental composition [21, 22]. For ternary alloys, we estimate the alloy crystal structure, the T_M, Curie temperature (T_C), and saturation magnetization (M_S) based upon the *e/a*-ratio [23]. The *e/a*-ratio describes the arithmetic average of the valence electrons surrounding each atom. Given plethora of previous literature, it is well known that increasing *e/a* increases T_M, but decreases T_C and M_S. Predictions of the stable phase are based upon the *e/a*-ratio, with 10M structure forming at *e/a* between 7.62 and 7.68, 14M forming between 7.68 and 7.72, and NM forming above 7.72 [23–26]. However, the boundaries between these structures are indistinct.

Effects of alloying Ni–Mn–Ga with Fe [19, 27–37], Cu [19, 35, 37–50], Co [19, 29, 30, 37–40, 43, 49, 51–53], and other transition elements [29, 37] have been subject of study. Additions of these elements change crystal structure, T_M, T_C, and M_S. Less explored is the combined effect of alloying elements with potential synergism. Synergistically, Co and Cu, alloyed at 4% into Ni–Mn–Ga allowed for the first magnetically induced reorientation for non-modulated MSM alloy: Co decreased tetragonality, while Cu increased martensite T_M [49], opening a new avenue in the MSM field.

We hypothesized that a synergism exists for alloying Cu and Fe combined into Ni–Mn–Ga for 10M phase. The addition of iron increases T_C [19, 40]. The addition of copper increases T_M, but also may decrease T_C [46]. We sought alloys to look for synergism of Fe and Cu in 10M phase to improve overall functional properties. While we did not find a clear synergism between the elements, we identified systematic trends between alloying elements and thermal and structural properties that differ from the trends of these elements in quaternary alloys (i.e., Ni–Mn–Ga-X, where X is Fe or Cu). Ni–Mn–Ga alloys with two additional elements have been challenging to understand, with the *total e/a* not serving alone as a predictor of behavior. We found a useful predictor to describe some systematic trends, the *elemental e/a*, that when used in combination with *total e/a*-ratio can help design of improved functional property MSM alloys.

Experimental

Alloy Design

We made eighteen Ni–Mn–Ga–Fe–Cu alloys and varied constituent elements around base system $Ni_{50}Mn_{28}Ga_{22}$. The alloy compositions (in at.%) are reported in Table 1. The alloys were designed to sweep several design constraints predicted to be important: keeping Ni (Mn) near 50% (28.5%); altering the Fe to Cu ratio (*Fe/Cu*). We swept a broad *total e/a* range, and additionally looked at systems with Mn 25 at.%. The alloys approximately follow:

Group 1	Ni 50%|Mn 25%|1–4% Fe and Cu at 1:1 Fe/Cu reducing Ga
Group 2	Ni 48%|Mn 28–31%|Fe 0–5% + Cu 1% reducing Ga, increasing *Fe/Cu*
Group 3	Ni 46.5% + Fe 3% | Mn 25–29% + Cu 1%, 2%, 3% reducing Ga
Group 4	Ni 49%|Mn 27–29%|Fe 3% & Cu 1–3% reducing Ga, high *e/a*

However, understanding exact group delineation is not necessary to understand the subsequent analysis. The reason for the grouping is mostly for discussion of the different preparation techniques applied for different groups.

Alloy Preparation and Measurements

Group 1 and 2 samples were prepared by arc melting pure metals under 4×10^{-4} mbar argon atmosphere with an Edmund Bühler MAM-1 arc furnace in a water cooled-copper crucible. Ingots were re-melted three times for homogeneity. Group 1 samples were annealed in an alumina crucible within a tube-furnace under argon gas flow at 1273 K for 72 h and ordered at 1073 K for 24 h, then left in the furnace to cool slowly. This treatment resulted in 3% Mn loss. Group 2 samples were annealed instead in argon-backfilled quartz ampoules and experienced $< 0.5\%$ Mn loss.

We prepared Groups 3 and 4 alloys differently. We weighed elements into 2 ml alumina crucibles and sealed them in argon-backfilled quartz ampoules. We melted alloys in a box furnace (Classic) at 1443 K for 48 h, then annealed and ordered following above alloying parameters. We checked homogeneity of alloys 7, 15, and 17 by sectioning the ingot into top, middle and bottom samples (A, B, C) and measured elemental composition by X-ray fluorescent spectroscopy with an Eagle III EDAX μProbe (XRF). The measurement error of the XRF was highest for the manganese and gallium compositions which was ± 0.5 at.%. The chemical segregation of Groups 3 and 4

Table 1 Composition, magnetic, and thermal properties of alloys: alloy grouping, alloy labeling, chemical compositions, martensitic transformation temperature T_M, Curie temperature T_C, saturation magnetization M_S, *total e/a*, and observed structure at $T = 250$ K

Group	Alloy	Composition [at.%]					T_M [K]	T_C [K]	2.0 T M_S [Am^2/Kg] 10 K	*e/a*	Structure 250 K
		Ni	Mn	Ga	Fe	Cu					
	1	50.4	24.8	21.7	1.4	1.7	347	369	58	7.73	NM
1	2	50.0	24.7	20.3	2.4	2.7	385	400	69	7.82	NM
	3	49.2	23.7	18	4.3	4.7	523	372	74	7.99	NM
	4	48.1	27.5	23.6	0	0.9	230	377	84	7.52	A
2	5	48.1	30.7	17.8	2.7	0.7	286	385	76	7.79	10M/A
	6	47.4	30.9	16.0	4.9	0.8	336	385	69	7.86	14M
	7A	46.4	24.9	24.6	3.2	0.9	162	388	90	7.48	A
	7B	46.5	24.7	24.7	3.2	0.9	160	386	85	7.48	A
	7C	46.2	24.9	24.8	3.3	0.9	159	387	86	7.46	A
	8	46.3	26.8	22.8	3.2	0.8	223	380	83	7.54	A
	9	46.2	29.1	20.6	3.3	0.9	290	369	73	7.54	10M
	10	46.7	24.5	23.8	3.2	1.8	158	419	86	7.55	A
3	11	46.2	26.8	21.9	3.2	1.9	222	390	83	7.62	A
	12	46.1	28.9	19.8	3.3	1.9	293	378	71	7.70	10M
	13	46.2	24.8	22.7	3.3	3.0	182	417	78	7.63	A
	14	46.0	26.9	20.8	3.2	3.0	247	388	73	7.70	10M/A
	15A	47.0	28.3	18.3	3.3	3.0	323	375	63	7.83	14M
	15B	46.9	28.1	18.8	3.3	3.0	344	373	60	7.81	14M
	15C	46.8	28.1	18.7	3.1	3.3	342	374	59	7.82	14M
	16	49.1	24.8	21.5	3.7	0.9	307	392	75	7.69	10M
	17A	49.1	27.1	18.7	3.2	2.0	413	385	60	7.84	NM
4	17B	49.3	27.0	18.5	3.2	2.0	413	385	53	7.85	NM
	17C	49.1	27.0	18.6	3.3	1.9	414	385	63	7.84	NM
	18	49.3	29.1	15.5	3.3	2.8	564	277	36	8.0	NM

alloys was at most 0.3%. Given their relatively homogenous nature, we just measured the center section of each ingot for the rest of alloys in these groups. The small variation in Mn concentration was within the typical range reported for annealed Ni–Mn–Ga alloys [54].

Wire electric discharge machining (ZAP BP) was used for sample cutting. The surfaces of all samples were ground with progressively finer grit SiC papers to 4000 grit for surface analysis to remove kerfs formed during discharge cutting and brass contamination from cutting wire. We determined crystal structures for the alloys with X-ray diffraction (XRD) using a PANalytical X'Pert PRO with Co and Cu tubes equipped with a cooling stage enabling cooling to 250 K.

Saturation field (2.0 T) and low-field (0.01 T) magnetizations as a function of temperature were measured using a vibrating sample magnetometer (Quantum Design PPMS) with temperature rate 4 K/min. The Curie temperature was determined from the inflection point of the low-field magnetization. The M_S was obtained at 10 K from the 2.0 T magnetization. For alloys with T_M greater than T_C, we used differential thermal analysis and differential scanning calorimetry (DTA/DSC), measured using a Setaram Setsys Evolution, in a helium gas flow with a 10 K/min ramp rate in the range 320–1140 K on heating and cooling.

The martensitic transformation was identified from the low-field magnetization data up to 400 K (i.e., for alloys 4–16), where we reported T_M as the average of the austenite and martensite start temperatures. Above 400 K, the extended high temperature range of the DSC calorimeter allowed better definition of NM structure alloys (i.e., for alloys 1–3, 17 and 18). Here T_M was the average between centers of the endothermic and exothermic peak.

Precise comparison between DTA and PPMS measurements is difficult, as differences arose from the placement of the thermocouple in relation to sample, the sample size, and the size of the sample chamber. These factors led to slightly different lag between the measured sample

temperatures vs. measured phenomena, as the heat-transfer conditions were different. We removed this lag from PPMS data by making the T_C coincident on heating and cooling. We also verified on the DSC data that the T_C extracted was consistent on heating and cooling. However, in this case the difference was about 5 K on heating and cooling.

Where Curie transitions were detected in both DSC and low-field magnetization measurements (in case of Alloy 17), the extracted martensitic transformation temperature agreed within 7 K, indicating good compatibility of the techniques and fairly low error. This is similar to the difference of around 5 K as reported in previous work by Chernenko et al. [55].

Element Contribution to *e/a*

For *total e/a* calculation, we used Ni, Mn, Ga, Fe, and Cu valence electron contributions of 10, 7, 3, 8, 11 electrons, respectively [50]. To find trends amid *e/a* data scatter, we introduced a new parameter, the *elemental e/a contribution*. The parameter differs from the *total e/a*-ratio. The *elemental e/a contribution* X_{element} compares the valence electrons associated with an element constituent to the *total e/a* of the alloy, separating elemental character from the change in overall *e/a*: $X_{\text{element}} = \frac{F_{\text{element}} \cdot E_{\text{element}}}{\sum f_i \cdot e_i}$, where F_{element} is atomic fraction of the element, E_{element} is the number of the element's valence electrons and the denominator is the *total* number of valence electrons per formula unit, which is just the *total e/a*

Consider 100 atoms of Ni_2MnGa. Fifty atoms are Ni, which each contribute 10 valence electrons (v.e.). Twenty-five Mn atoms contribute each 7 v.e.; twenty-five Ga atoms each contributes 3 v.e. In total, the one-hundred atoms have 750 total v.e., of which Ni, Mn, and Ga contribute 66.7%, 23.3%, and 10.0% to the *total e/a*, i.e., $X_{Ni} = 0.667$, $X_{Mn} = 0.233$, $X_{Ga} = 0.100$. For $Ni_{50}Mn_{28}Ga_{22}$, $X_{Ni} = 0.656$, $X_{Mn} = 0.257$, $X_{Ga} = 0.087$.

Results

The XRD analysis indicated the presence of the common martensite phases (NM, 14M and 10M) and cubic austenite in samples (Table 1). A mixture of multiple phases was detected for samples in the as-cast state, but after annealing samples became largely single phase. All the samples were highly textured polycrystals with (100) type reflections distributed in a small range of Euler angles. Annealing did not broaden the range. In alloys 7–18 larger grains were detected based on distinct spots in the XRD pole figures (not shown). This difference can be ascribed to the different manufacturing methods with different thermal gradients. For these alloys, the material appeared to be oligo-crystalline rather than polycrystalline.

Results from the PPMS, DTA and XRD measurements were compiled into Table 1. The melting temperature was measured in alloys 1–3, 17, 18. The melting temperature was between 1363 and 1384 K. The B2′-$L2_1$ ordering temperature was between 973 and 1017 K.

Figure 1 shows the measured T_M, T_C, and M_S data from Table 1, plotted against *total e/a.* Lines were drawn to compare to the Chernenko [23] ternary system T_M, T_C, and M_S, where the martensitic temperature was determined using DSC [55]. The difference between the two methods is, as previously stated in "Alloy Preparation and Measurements" section as around 5–7 K, given sharp transformation behavior.

Figure 2 shows T_M plotted against *elemental contribution to e/a* (X_{Ni}) from Eq. 1. Here we note these trends: alloys in the upper circled region had NM structure, while alloys in the lower circled region had 10M/14M structure. NM structure tended to form with increased X_{Ni} and with high *total e/a*. Modulated structures formed with decreased X_{Ni} and lower *total e/a*. Alloys in Groups 1 and 4 were NM, while Group 2 alloys fell in the lower ellipse region and had modulated structure. The solid line indicates T_M behavior for the Group 3 alloys which approximately followed $Ni_{46.5}Mn_{25+X}Ga_{25-X-Y}Fe_{3.5}Cu_Y$ (i.e., Ni and Fe add up to $\sim$ 50 at.%) alloying, and is the system analyzed further in Figs. 4, 5 and 6. Alloy 6 also fell along the solid line, but had higher Ni concentration than Group 3 alloys, and is not included in the Group 3 analysis. The red dashed line indicates the T_M versus X_{Ni} for Ni–Mn–Ga, back-

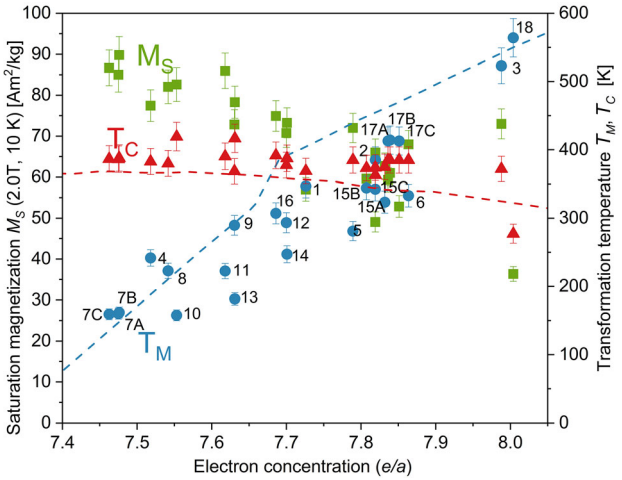

Fig. 1 Martensite transformation temperatures and Curie temperatures T_M, T_C, and saturation magnetization M_S as functions of *e/a* in Ni–Mn–Ga–Fe–Cu alloys and previously reported *e/a* trends (dashed lines) for ternary alloys from [23]. T_M, T_C, and M_S values are plotted as as blue circles, red triangles, and green squares, respectively. The blue dashed line shows the ternary system T_M; the red dashed line shows the ternary system T_C (Color figure online)

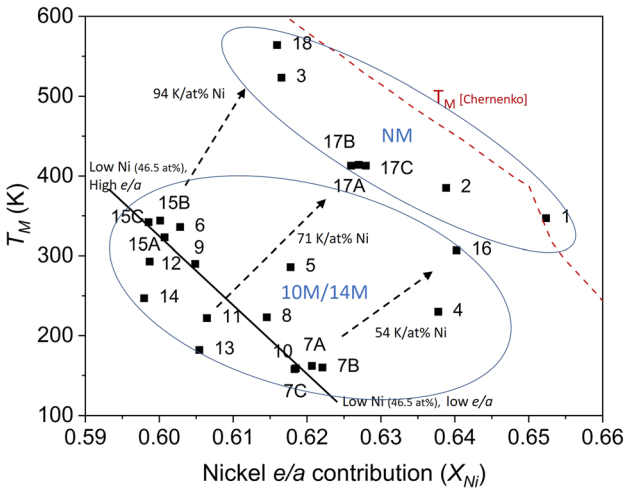

Fig. 2 Martensite transformation temperature as a function of X_{Ni}. Alloy labels are from Table 1. Alloys in the upper and lower ellipse have the NM and modulated structures. The red dashed line indicates X_{Ni} contribution of Ni–Mn–Ga calculated from [23]. The solid black line marks alloys following $Ni_{46.5}Mn_{25+X}Ga_{25-X-Y}Fe_{3.5}Cu_Y$. We compared alloys along the black line with alloys in the NM region, which differ in Ni and Ga. The rate of increase between alloys is marked with a dashed arrow

calculated from [23] in which Ni concentration is 50% [23]. The back-calculated values were compared to data from Sozinov et al. [21], which closely follow Ref.[23], but do not indicate the inflection region reported by Chernenko [23]. The dashed arrows indicate the systematic increase in T_M with increasing Ni alloying discussed "Effect of nickel on T_M" section.

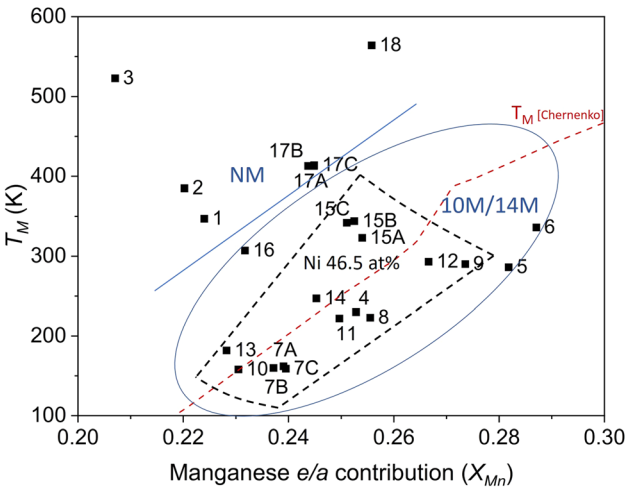

Fig. 3 Martensitic transformation temperatures as a function of X_{Mn}. Alloys above the solid line had the NM structure. Alloys within the blue ellipse have modulated structure. The red dashed line indicates X_{Mn} contribution of Ni–Mn–Ga calculated from [23]. The black dashed lines enclose a region where systematic trends are found and further noted in Fig. 4

In Fig. 3 we plotted T_M as a function X_{Mn}, and also T_M for Ni–Mn–Ga calculated from Chernenko [23]. The upper solid line delineates NM from modulated structure. Alloys with high Ni content (Group 1 and 4 alloys) had high T_M, but were NM structure with increased Fe and Cu alloying. Alloys with lower Ni content (Group 2 and 3 alloys) were within the region marked by an ellipse and had modulated structure. In these alloys, T_M increased with increasing X_{Mn} and maintained modulated structure up to $X_{Mn} \sim 0.29$; X_{Mn} above this was outside the scope of this study. The dashed region marks Group 3 alloys which had close to 46.5 at.% Ni and 3.5 at.% Fe and were further analyzed in Figs. 4, 5 and 6. Some Group 2 alloys fell within the dashed region of Fig. 3, but had higher Ni than Group 3 alloys, and had properties in-between high Ni content (Groups 1 and 4) and low Ni content (Group 3) alloys.

Figure 4 compares in detail T_M of Group 3 alloys against X_{Mn}. T_M increased with Mn content following contours marked in blue solid lines of constant Mn concentration. We identified contours of constant Cu concentration and marked these as solid green lines. From the Mn and Cu concentration contours, we isolated Mn and Cu effects upon T_M from the overall convolution of the effects of the other elements. We plotted also T_M against X_{Mn}, calculated from [23] as the dashed red line to note the location and slope of the ternary line vs that for the quinary alloys.

Figure 5 compares M_S of Group 3 alloys against X_{Cu}. Alloys with similar X_{Cu} were marked along solid green lines of constant Cu concentration. X_{Cu} was from 0.045–0.05, i.e., was quite small, which caused X_{Cu} to align

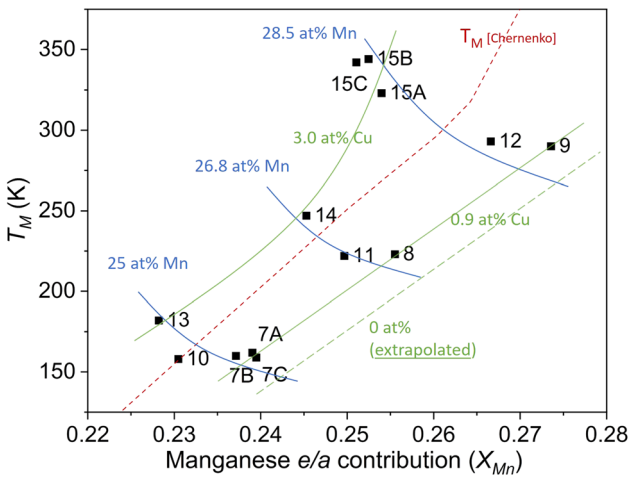

Fig. 4 Systematic trends in the $Ni_{46.5}Mn_{25+X}Ga_{25+X-Y}Fe_{3.5}Cu_y$ system lying within the area bound with a dashed line in Fig. 3. Contours of constant Mn (Cu) concentration are marked with blue (green) solid lines. The reference X_{Mn} contribution retrieved from Chernenko [23] is plotted in a red dashed line. A zero copper line extrapolated from the data of this study is marked with a green dashed line (Color figure online)

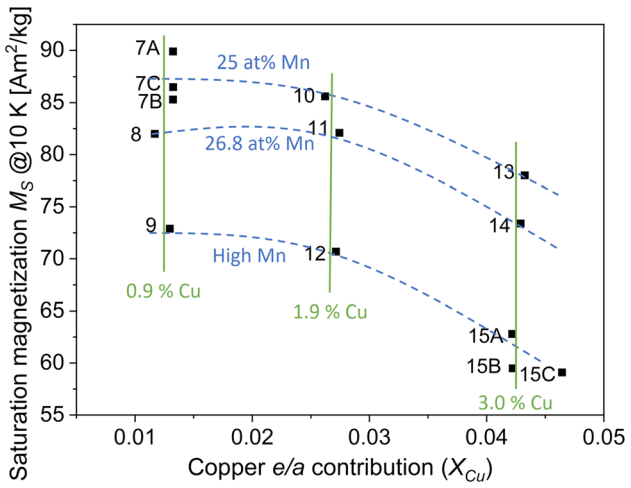

Fig. 5 Saturation magnetization plotted against X_{Cu} for the $Ni_{46.5}Mn_{25+X}Ga_{25+X-Y}Fe_{3.5}Cu_Y$ system. Green solid line marks alloys with constant Cu concentration. Dashed blue lines indicate contours of constant Mn concentration (Color figure online)

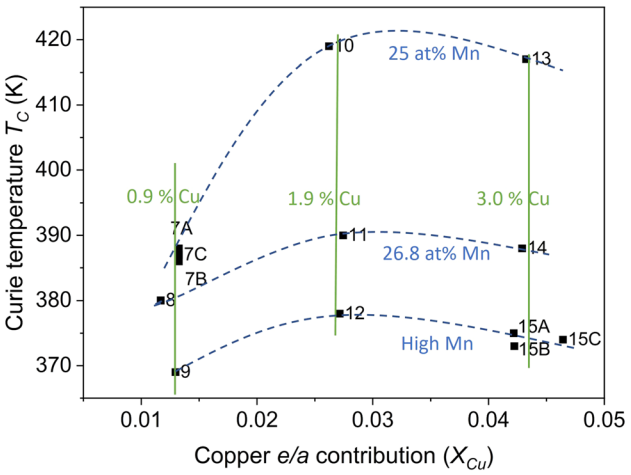

Fig. 6 Curie temperature plotted against X_{Cu} for the $Ni_{46.5}Mn_{25+X}Ga_{25-X-Y}Fe_{3.5}Cu_Y$ system. Solid green (dashed blue) lines indicate contours of constant Cu (Mn) concentration (Color figure online)

predominantly vertical irrespective of *total e/a*. The dashed blue lines indicated M_S for Mn content of 25 at.% and 26.8 at.% and for higher Mn (28.1–29.1 at.%). We found systematic contours which show the coefficient of decreased M_S with increased Mn and Cu alloying.

In Fig. 6, we plotted for Group 3 alloys the Curie temperature against X_{Cu}. Alloys with common Cu concentration aligned in vertical contours and were marked as green solid lines. The trend in Curie temperature for constant Mn concentration was drawn in dashed blue lines.

Discussion

Analysis of *Total e/a*

Compared to the ternary Ni–Mn–Ga system, the *total e/a* diagram (Fig. 1) shows approximately 100 K scatter in martensitic transformation temperatures for a given *e/a*. The large scatter indicates that the *total e/a*-ratio is not effective in predicting transformation temperatures for Ni–Mn–Ga–Fe–Cu. The intersection line reported by Chernenko [23] turns into a broad intersection range that extends from *total e/a* $\sim$ 7.72 to 7.88 (Fig. 1).

In ternary Ni–Mn–Ga alloys, increasing *total e/a* above 7.7 results successively in formation of the 14M and NM structure [22]. In quaternary Ni–Mn–Ga alloys singularly alloyed with either Cu or Fe the *e/a* for 10M structure have been as high as 7.82 for alloy $Ni_{50}Mn_{25}Ga_{21}Cu_4$ [56]. In this study, the maximum *total e/a* found for 10M was in Alloy 5, which had 7.79 with T_M = 286 K. The maximum *e/a* found for 14M alloy was 7.83 in Alloy 15. In all cases, transformation temperatures for Ni–Mn–Ga–Fe–Cu are less than those found for well-annealed ternary alloys, despite having higher *total e/a*. Alloys on upper T_M spread are near to Ni–Mn–Ga compositions (Alloy 4), they have lower nickel and some iron, but little copper. Alloys on the lower T_M band have high Cu, or high Mn and more substantial Fe or Cu, but these trends are neither obvious, nor systematic.

Effect of Nickel on T_M

In Fig. 2 we look at nickel according to its *elemental e/a*. Ni is second only to Cu in number of valence electrons, and its elemental *e/a* contribution is large. In Fig. 2, outside of the Group 3 alloys (bottom solid line), Ni appeared the dominant factor in T_M. Alloys with high X_{Ni} and high *total e/a* had NM structure.

To isolate the effect of Ni we compare alloys which vary only by Ni and Ga. Alloy 7 and Alloy 16 have almost equivalent composition, with varying Ni and Ga concentration (Table 1). The coefficient of increasing T_M by increasing Ni content is 54 K/at.% Ni at Mn 25 at.%. The coefficient from increasing Ni content between alloys 11 and 17 is 71 K/at.% Ni at Mn 27 at.%. The coefficient from increasing Ni content between alloys 15 and 18 is masked by the Mn increase, but if we assume a dependence of T_M of 30 K/at.% Mn (found in subsequent "Mn effects on T_M" section), the coefficient due to the increase of Ni content is 94 K/at.% Ni at 28 at.%. The rates are noted upon Fig. 2 as dashed arrows marking the transformation path.

Alloys with high Mn content have a larger Ni coefficient of T_M increase, which causes transformation to 14M

structure. Some results suggest Fe acts similarly as Ni, as systematic trends were found for the combined Ni and Fe adding to 50%, with slope parallel to that of the ternary system reported by Chernenko [23], with Mn and Cu varying.

Group 3 Alloys: Analysis of Manganese and Copper on T_M

Alloys in Group 3 approximately follow $Ni_{46.5}Mn_{25+X}Ga_{25-X-Y}Fe_{3.5}Cu_Y$ alloying which is the system indicated in Fig. 2 as the lower solid line and within Fig. 3 as the dashed region. In this system with the fixed Ni and Fe content, T_M varies systematically with Cu concentration along contours of constant Mn concentration. Along the blue contours, T_M increases as Cu substitutes for Ga. Along the green contours, Cu remains constant while Mn replaces Ga.

Cu Effects on T_M

Referring to Fig. 4 and comparing to Table 1, along the constant 25% Mn concentration contour, alloys 7 and 13 vary by 2% Cu concentration and replaced Ga. The increase of 2% Cu content causes an increase of 20 K in T_M, with a coefficient of 10 K/at.% Cu. Along the 26.8% Mn concentration contour, comparing Alloys 8 and 14, T_M increases at 11 K/at.% Cu. Along the 28.5% Mn concentration contour, comparing alloys 9 and 15, the Cu effect is obscured by varying Mn content, but if we use a 30 K/at.% Mn dependence (from subsequent section), we find the corrected coefficient to be 9 K/at.% Cu. Thus, despite the shift to the 14M structure, the T_M coefficient remains the same.

Comparing this quinary system to previous results of quaternary alloys, Glavatskyy et al. [50] found 10M structure in $Ni_{49.4}Mn_{23.3}Ga_{25.6}Cu_{1.7}$ with $T_M \sim 337$ K. Our closest alloy to this is Alloy 1, which is, however, NM structure. Glavatskyy et al. found another 10M alloy at $Ni_{47.3}Mn_{25.5}Ga_{24.5}Cu_{2.7}$ with $T_M \sim 335$ K. The closest composition was our Alloy 10, which likely has 10M martensitic structure owing to low transforming temperature (158 K), but was austenitic within measurable range of our XRD set-up.

Mn Effects on T_M

Applying the same method to Mn: if we compare alloys 7 and 8 from Table 1, which both lie on the 0.9% Cu concentration contour (Fig. 4) we find Mn increases T_M by 32 K/at.% Mn. We find that, between alloys 8 and 9, the T_M increase is 30 K/at.% Mn. Between alloys 13 and 14, the coefficient is 31 K/at.% Mn. Along the constant 28.5% Mn concentration contour, replacing Ga with Cu shifts the structure to 14M. Between alloys 14 and 15C, the coefficient increases to 79 K/at.% Mn. The increased coefficient seems to be due to the phase transformation. The cause of the structural transformation to 14M might be due to specific Cu elemental effects, or from the extra *total e/a added by* Cu, or both.

Comparison to Ternary System and Quaternary Systems

For Group 3 alloys we found Mn had a larger coefficient than Cu with increased T_M, despite having a lower concentration of valence electrons (i.e., lower *total e/a*). The coefficient is constant in the 10M region, but changes as the material changes structure. Alloy T_M varies systematically with both Cu and Mn, but with three times greater rate for Mn addition.

The Ni–Mn–Ga–Fe–Cu T_M dependence upon Mn concentration is similar to that from Chernenko who found a slope 37.5 K/at.% Mn in the 10M region [23]. Extrapolating the contours of constant Mn concentration to zero Cu concentration, T_M is decreased compared to the ternary system, which might be attributed to adding Fe at Ni expense. Replacing Ni with Fe, though, allows for increased Mn content, which can lead to alloys with reasonably high T_M (Alloy 9). The 10M structure was found in alloys with high Mn with some Fe replacing Ni. This is also seen in Guldbakke et al. [34] in $Ni_{45.4}Mn_{29.1}Ga_{21.6}Fe_{3.9}$ with $T_M = 323$ K.

Effect of Iron on T_M

Iron has a less clear impact on T_M. When we compare Alloys 5 and 6, which vary mostly in Fe and Ga content, but also slightly in Ni content; the 2.2% Fe increases T_M by 50 K for a coefficient of 23 K/at.% Fe. However, Ni content also decreased by 0.7%, which, assuming the middle Ni rate of 71 K/at.% Ni, would indicate that increasing Fe content actually increased T_M by 73 K/at.% Fe. This number may be taken only perfunctorily, as the data set is limited. In Fig. 4, by extrapolating T_M to zero Cu, when Fe replaces Ni, T_M decreased compared to the ternary system. Obtained data suggest 10M structure may be found systematically when adding Fe at Ni expense.

Saturation Magnetization (M_S)

In Fig. 1, plotted against the *total e/a*-ratio, M_S decreases generally, but not systematically with increasing *e/a*. In Fig. 5, we plot M_S for Group 3 alloys against X_{Cu}. The alloys group into vertical contours of constant X_{Cu}, with M_S varying systematically according to Mn concentration. For constant Cu concentration, M_S decreases with increasing

Mn. Given a low Cu content, the number of participating valence electrons would be small, such that just chemical composition well approximates the elemental contribution. Nonetheless, the data showed better fit to the electron-weighted *elemental e/a contribution*.

Effects of Mn on M_S

Along the line of fixed 0.9% Cu concentration, comparing alloys 7 and 9 with increasing Mn concentration, M_S decreases at coefficient 2.8 (Am^2/kg)/at.% Mn. Along the line of fixed 3% Cu concentration, comparing alloys 13 and 15, increasing the Mn concentration decreases M_S by 5.1 (Am^2/kg)/at.% Mn.

Effects of Cu on M_S

Given constant 25 at.% Mn concentration, comparing alloys 7 and 13, the increase in Cu concentration decreases M_S at 2.8 (Am^2/kg)/at.% Cu. Comparing alloys 9 and 15 with high Mn concentration, the trend is less clear, as the Mn concentration also increases slightly, but, after removing the Mn dependence, we find that increasing Cu concentration decreases M_S at 3.3 (Am^2/kg)/at.% Cu.

Mn alloyed in excess of 25 at.% decreased M_S, which can be ascribed to Mn atoms occupying Ga sites and coupling anti-ferromagnetically to Mn on Mn sites, which decreases the overall magnetic moment [57, 58]. Increasing Cu content decreased M_S at slightly less than the Mn coefficient, indicating that some Cu atoms occupy Mn sites.

Curie Temperature

Plotting against X_{Cu}, T_C systematically decreases with Mn concentration, but does not monotonously vary with the Cu concentration. There is unexpectedly large change in T_C between alloy 7 and alloy 10, which might indicate an effect of low Cu, which we attribute to annealing uncertainty or another unknown effect at low *e/a*. Between the 25% and 26.8% Mn concentration contours, the coefficient was 3.7 K/at.% Mn from alloy 7 to alloy 8, and 14 K/at.% Mn between alloys 13 and 14. The coefficient was less for higher Mn concentrations: when comparing 26.8 at.% Mn to 28.1–29.1 at.% Mn, the coefficient was 4.8 K/at.% Mn between alloys 8 and 9, and 9.3 K/at.% Mn between alloys 14 and 15. With Ni, Fe, and Mn concentrations held constant, increasing Cu concentration at Ga expense in some cases actually increased T_C, as found when comparing alloys 7 and 10. Adding Fe did not appear to increase T_C temperatures substantially.

New Questions

This phenomenological study evaluated the impact of Cu and Fe on the phase transformation temperatures and structure of quinary Ni–Mn–Ga–Fe–Cu alloys. We found that the elements Fe and Cu have different effects when alloyed together than when alloyed individually in quinary Ni–Mn–Ga-X alloys. Researchers may employ density functional theory calculations to understand such differences.

Conclusions

With original intent to create a new, high temperature MSM alloy, we realized a need for new methods to evaluate the broad range of experimental data. We developed a method based on the *individual* contribution of each element to the *total e/a*-ratio. Using this *elemental e/a contribution,* we found coefficients which describe alloying of Ni, Mn, and Cu upon T_M, M_S, and T_C. Our experiments indicated that Ni has the largest T_M coefficient, followed by Mn and Cu. Mn additions decreased saturation magnetization at a similar coefficient as Cu alloying. Mn addition systematically decreased the Curie temperature, while Cu had unsystematic effect, even increasing the Curie temperature in cases. Comparison of the slope of the $Ni_{46.5}Fe_{3.5}$ system to ternary system suggests that Fe might act similarly to Ni in the quinary system. The 10M martensite structure is stable for the composition $Ni_{46.5}Mn_{25+X}Ga_{25-X-Y}Fe_{3.5}Cu_Y$ where X and Y range from 0.9 to 4 and from 1 to 3. Using both the *elemental* and *total e/a-ratios* gives some insight into the complex behavior of quinary MSM alloys, which can be useful for a consideration of MSM alloys with improved functional properties.

Acknowledgements We acknowledge the support of Czech Science Foundation (grant No. 16-00043S). We also acknowledge the support of Operational Program Research, Development and Education financed by European Structural and Investment Funds and the Czech Ministry of Education, Youth and Sports (Project SOLID21-CZ.02.1.01/0.0/0.0/16_019/0000760 and MATFUN-CZ.02.1.01/0.0/0.0/15_003/0000487). Initial compositional EDS measurements were conducted by Ladislav Klimša, and casting of some alloys was performed by Martin Dušák at FZU. Experiments were performed in MGML (https://mgml.eu), which is supported within the program of Czech Research Infrastructures (project no. LM2018096). PM acknowledges partial financial support through the National Science Foundation project DMR-1710640.

References

1. Ullakko K (1996) Magnetically controlled shape memory alloys: a new class of actuator materials. J Mater Eng Perform 5(3):405–409

2. Likhachev A, Sozinov A, Ullakko K (2006) Modeling the strain response, magneto-mechanical cycling under the external stress, work output and energy losses in Ni–Mn–Ga. Mech Mater 38(5–6):551–563
3. Aaltio I, Heczko O, Söderberg O, Hannula S (2009) Magnetically controlled shape memory alloys, smart materials. CRC-Press, Boca Raton, pp 20–1e20
4. Murray S, Marioni M, Kukla A, Robinson J, O'Handley R, Allen S (2000) Large field induced strain in single crystalline Ni–Mn–Ga ferromagnetic shape memory alloy. J Appl Phys 87(9):5774–5776
5. Smith AR, Tellinen J, Ullakko K (2014) Rapid actuation and response of Ni–Mn–Ga to magnetic-field-induced stress. Acta Mater 80:373–379
6. Kucza NJ, Patrick CL, Dunand DC, Müllner P (2015) Magnetic-field-induced bending and straining of Ni–Mn–Ga single crystal beams with high aspect ratios. Acta Mater 95:284–290
7. Ullakko K, Wendell L, Smith A, Müllner P, Hampikian G (2012) A magnetic shape memory micropump: contact-free, and compatible with PCR and human DNA profiling. Smart Mater Struct 21(11):115020
8. Barker S, Rhoads E, Lindquist P, Vreugdenhil M, Müllner P (2016) Magnetic shape memory micropump for submicroliter intracranial drug delivery in rats. J Med Dev 10(4):126–232
9. Aaltio I, Lahelin M, Söderberg O, Heczko O, Löfgren B, Ge Y, Seppälä J, Hannula S-P (2008) Temperature dependence of the damping properties of Ni–Mn–Ga alloys. Mater Sci Eng A 481:314–317
10. Nilsén F, Aaltio I, Hannula S-P (2018) Comparison of magnetic field controlled damping properties of single crystal Ni-Mn-Ga and Ni-Mn-Ga polymer hybrid composite structures. Compos Sci Technol 160:138–144
11. Feuchtwanger J, Richard ML, Tang YJ, Berkowitz AE, O'Handley RC, Allen SM (2005) Large energy absorption in Ni–Mn–Ga/polymer composites. J Appl Phys 97(10):10M319
12. Heczko O, Kopecký V, Sozinov A, Straka L (2013) Magnetic shape memory effect at 1.7K. Appl Phys Lett 103(7):072405
13. Noda Y, Shapiro S, Shirane G, Yamada Y, Tanner L (1990) Martensitic transformation of a Ni-Al alloyi Experimental results and approximate structure of the seven-layered phase. Phys Rev B 42(16):10397
14. Murray S, Marioni M, Allen S, O'handley R, Lograsso TA (2000) 6% magnetic-field-induced strain by twin-boundary motion in ferromagnetic Ni–Mn–Ga. Appl Phys Lett 77(6):886–888
15. Sozinov A, Likhachev AA, Lanska N, Ullakko K (2002) Giant magnetic-field-induced strain in NiMnGa seven-layered martensitic phase. Appl Phys Lett 80(10):1746–1748
16. Jiang C, Liang T, Xu H, Zhang M, Wu G (2002) Superhigh strains by variant reorientation in the nonmodulated ferromagnetic NiMnGa alloys. Appl Phys Lett 81(15):2818–2820
17. Söderberg O, Straka L, Novák V, Heczko O, Hannula S-P, Lindroos V (2004) Tensile/compressive behaviour of non-layered tetragonal Ni52. 8Mn25. 7Ga21. 5 alloy. Mater Sci Eng A 386(1–2):27–33
18. Straka L, Hänninen H, Soroka A, Sozinov A (2011) Ni-Mn-Ga single crystals with very low twinning stress. J Phys 12:012079
19. Pérez-Checa A, Musiienko D, Saren A, Soroka A, Feuchtwanger J, Sozinov A, Barandiaran J, Ullakko K, Chernenko V (2019) Study of the critical parameters for magnetic field-induced strain in high temperature Ni-Mn-Ga-Co-Cu-Fe single crystals. Scr Mater 158:16–19
20. Pagounis E, Chulist R, Szczerba M, Laufenberg M (2014) High-temperature magnetic shape memory actuation in a Ni–Mn–Ga single crystal. Scr Mater 83:29–32
21. Sozinov A (2009) Low twinning stress Ni2Mn(1+X)Ga(1-X) alloys. ICFSMA, Bilbao
22. Heczko O, Straka L (2004) Compositional dependence of structure, magnetization and magnetic anisotropy in Ni–Mn–Ga magnetic shape memory alloys. J Magn Magn Mater 272:2045–2046
23. Chernenko VA (1999) Compositional instability of β-phase in Ni-Mn-Ga alloys. Scr Mater 40(5):523–527
24. Jin X, Marioni M, Bono D, Allen S, O'handley R, Hsu T (2002) Empirical mapping of Ni–Mn–Ga properties with composition and valence electron concentration. J Appl Phys 91(10):8222–8224
25. Pons J, Chernenko V, Santamarta R, Cesari E (2000) Crystal structure of martensitic phases in Ni–Mn–Ga shape memory alloys. Acta Mater 48(12):3027–3038
26. Chernenko VA, Seguí C, Cesari E, Pons J, Kokorin VV (1998) Sequence of martensitic transformations in Ni-Mn-Ga alloys. Phys Rev B 57(5):2659–2662
27. Soto-Parra D, Moya X, Mañosa L, Planes A, Flores-Zúñiga H, Alvarado-Hernández F, Ochoa-Gamboa R, Matutes-Aquino J, Ríos-Jara D (2010) Fe and Co selective substitution in Ni_2MnGa: Effect of magnetism on relative phase stability. Philos Mag 90(20):2771–2792
28. Soto D, Hernández FA, Flores-Zúñiga H, Moya X, Manosa L, Planes A, Aksoy S, Acet M, Krenke T (2008) Phase diagram of Fe-doped Ni-Mn-Ga ferromagnetic shape-memory alloys. Phys Rev B 77(18):184103
29. Glavatskyy I, Glavatska N, Söderberg O, Hannula S-P, Hoffmann J-U (2006) Transformation temperatures and magnetoplasticity of Ni–Mn–Ga alloyed with Si. In, Co or Fe, Scr Mater 54(11):1891–1895
30. Fayzullin R, Buchelnikov VD, Taskaev S, Drobosyuk M, Khovaylo VV (2013) Experimental Study of Magnetocaloric Effect in Ni-Fe-Mn-Ga and Ni-Co-Mn-Ga Heusler Alloys. Mater Sci Forum 738:456–460
31. Khovailo V, Chernenko V, Cherechukin A, Takagi T, Abe T (2004) An efficient control of Curie temperature TC in Ni–Mn–Ga alloys. J Magn Magn Mater 272:2067–2068
32. Yu S, Yan S, Kang S, Tang X, Qian J, Chen J, Wu G (2011) Magnetic field-induced martensite–austenite transformation in Fe-substituted NiMnGa ribbons. Scr Mater 65(1):9–12
33. Liu Z, Zhang M, Wang W, Wang W, Chen J, Wu G, Meng F, Liu H, Liu B, Qu J (2002) Magnetic properties and martensitic transformation in quaternary Heusler alloy of NiMnFeGa. J Appl Phys 92(9):5006–5010
34. Guldbakke J, Chmielus M, Rolfs K, Schneider R, Müllner P, Raatz A (2010) Magnetic, mechanical and fatigue properties of a Ni45. 4Mn29. 1Ga21. 6Fe3. 9 single crystal. Scr Mater 62(11):875–878
35. Barabash RI, Barabash OM, Popov D, Shen G, Park C, Yang W (2015) Multiscale twin hierarchy in NiMnGa shape memory alloys with Fe and Cu. Acta Mater 87:344–349
36. Koho K, Söderberg O, Lanska N, Ge Y, Liu X, Straka L, Vimpari J, Heczko O, Lindroos V (2004) Effect of the chemical composition to martensitic transformation in Ni–Mn–Ga–Fe alloys. Mater Sci Eng A 378(1–2):384–388
37. Guo S, Zhang Y, Quan B, Li J, Qi Y, Wang X (2005) The effect of doped elements on the martensitic transformation in Ni–Mn–Ga magnetic shape memory alloy. Smart Mater Struct 14(5):S236
38. Perez-Checa A, Feuchtwanger J, Musiienko D, Sozinov A, Barandiaran JM, Ullakko K, Chernenko VA (2017) High temperature Ni45Co5Mn25(-) xFexGa20Cu5 ferromagnetic shape memory alloys. Scr Mater 134:119–122
39. Pérez-Checa A, Feuchtwanger J, Musiienko D, Sozinov A, Barandiaran JM, Ullakko K, Chernenko VA (2017) High temperature Ni45Co5Mn25−xFexGa20Cu5 ferromagnetic shape memory alloys. Scr Mater 134:119–122

40. Perez-Checa A, Feuchtwanger J, Barandiaran J, Sozinov A, Ullakko K, Chernenko V (2018) Ni-Mn-Ga-(Co, Fe, Cu) high temperature ferromagnetic shape memory alloys: effect of Mn and Ga replacement by Cu. Scr Mater 154:131–133
41. Roy S, Blackburn E, Valvidares S, Fitzsimmons M, Vogel SC, Khan M, Dubenko I, Stadler S, Ali N, Sinha S (2009) Delocalization and hybridization enhance the magnetocaloric effect in Cu-doped Ni 2 MnGa. Phys Rev B 79(23):235127
42. Nicholson DM, Odbadrakh K, Shassere B, Rios O, Hodges J, Ludtka GM, Porter WD, Sefat A, Rusanu A, Brown G (2014) Modeling and characterization of the magnetocaloric effect in Ni2MnGa materials. Int J Refrig 37:289–296
43. Zelený M, Sozinov A, Straka L, Björkman T, Nieminen RM (2014) First-principles study of Co-and Cu-doped Ni 2 MnGa along the tetragonal deformation path. Phys Rev B 89(18):184103
44. Zeleny M, Sozinov A, Bjorkmand T, Straka L, Nieminen RM (2015) Ab initio study of properties of Co- and Cu- doped Ni-Mn-Ga alloys. Mater Today 2:601–604
45. Li Y, Wang J, Jiang C (2011) Study of Ni–Mn–Ga–Cu as single-phase wide-hysteresis shape memory alloys. Mater Sci Eng A 528(22–23):6907–6911
46. Tan C, Dong G, Gao L, Sui J, Gao Z, Cai W (2012) Microstructure, martensitic transformation and mechanical properties of Ni50Mn30Ga20−xCux ferromagnetic shape memory alloys. J Alloys Compd 538:1–4
47. Aaltio I, Söderberg O, Friman M, Glavatskyy I, Ge Y, Glavatska N, Hannula S (2009) Determining the liquidus and ordering temperatures of the ternary NiMn-Ga and quaternary Ni-Mn-Ga-Fe/Cu alloys. EDP Sciences, European Symposium on Martensitic Transformations, p 04001
48. Rameš M, Heczko O, Sozinov A, Ullakko K, Straka L (2018) Magnetic properties of Ni-Mn-Ga-Co-Cu tetragonal martensites exhibiting magnetic shape memory effect. Scr Mater 142:61–65
49. Sozinov A, Lanska N, Soroka A, Zou W (2013) 12% magnetic field-induced strain in Ni-Mn-Ga-based non-modulated martensite. Appl Phys Lett 102(2):021902
50. Glavatskyy I, Glavatska N, Dobrinsky A, Hoffmann JU, Söderberg O, Hannula SP (2007) Crystal structure and high-temperature magnetoplasticity in the new Ni–Mn–Ga–Cu magnetic shape memory alloys. Scri Mater 56(7):565–568
51. Fabbrici S, Porcari G, Cugini F, Solzi M, Kamarad J, Arnold Z, Cabassi R, Albertini F (2014) Co and In doped Ni-Mn-Ga magnetic shape memory alloys: a thorough structural, magnetic and magnetocaloric study. Entropy 16(4):2204–2222
52. Chatterjee S, Giri S, De S, Majumdar S (2010) Giant magnetocaloric effect near room temperature in Ni–Mn–Sn–Ga alloys. J Alloys Compd 503(2):273–276
53. Nicholson DM, Odbadrakh K, Rusanu A, Eisenbach M, Brown G, Evans I (2011) Boyd Mccutchen, First principles approach to the magneto caloric effect: application toNi2MnGa. J Appl Phys 109(7):07A942
54. Nilsén F, Aaltio I, Ge Y, Lindroos T, Hannula S-P (2015) Characterization of gas atomized Ni-Mn-Ga powders. Mater Today 2:S879–S882
55. Chernenko V, Cesari E, Kokorin V, Vitenko I (1995) The development of new ferromagnetic shape memory alloys in Ni-Mn-Ga system. Scr Metall Mater 33(8):1239–1244
56. Santamarta R, Muntasell J, Font J, Cesari E (2015) Thermal stability and microstructure of Ni–Mn–Ga–Cu high temperature shape memory alloys. J Alloys Compd 648:903–911
57. Lázpita P, Barandiarán J, Gutiérrez J, Feuchtwanger J, Chernenko V, Richard M (2011) Magnetic moment and chemical order in off-stoichiometric Ni–Mn–Ga ferromagnetic shape memory alloys. New J Phys 13(3):033039
58. Enkovaara J, Heczko O, Ayuela A, Nieminen R (2003) Coexistence of ferromagnetic and antiferromagnetic order in Mn-doped Ni2MnGa. Phys Rev B 67(21):1–4